



*Int. J. New. Chem., 2021, Vol. 8, Issue 4, pp. 425-441.*

## International Journal of New Chemistry

Published online January 2021 in <http://www.ijnc.ir/>.

Open Access

Print ISSN: 2645-7236

Online ISSN: 2383-188x



Article Type (Review Article or Original Research Article or Short Communication)

### A density functional theory study on nanostructures including sumanene, corannulene and nanosheet as the anodes in Be-ion Batteries

Fatemeh Gharibzadeh<sup>1</sup>, Esmail Vessally<sup>2</sup>, Ladan Edjlali<sup>1,\*</sup>, Moosa Es'haghi<sup>1</sup>, Robab Mohammadi<sup>2</sup>

<sup>1</sup> Department of Chemistry, Tabriz Branch, Islamic Azad University, Tabriz, Iran

<sup>2</sup> Department of Chemistry, Payame Noor University, Tehran, Iran

Received: 2021/03/17

Accepted: 2021/06/19

Published: 2021/09/15

#### ABSTRACT

A theoretical study were performed to examine the interactions between the Be neutral atom and Be<sup>2+</sup> ion and three sheet-Like nanoparticles such as sumanene (SM), corannulene (CN) and graphene, which are computed by M06-2X/6-31+G(d,p) method. The estimated values of adsorption energy ( $E_{ad}$ ) are all negative in Be<sup>2+</sup>-nanoparticles interaction. These results can be understood in terms of the electrostatic potentials of the negative sites on nanoparticles with which the positive regions on the Beryllium ion are interacting. In this article, the cell voltage (V) is the most important parameter for Be-ion batteries. It also determines the usability of a battery in an electrical system, and many battery parameters depend on voltage. Nevertheless, the  $V_{cell}$  for CN was obtained the highest value. The  $V_{cell}$  of Be-ion batteries are increased in the order: CN > SM > graphene > SM-i > CN-i. The mentioned nanoparticles as the anodes in BeIBs.

**Keywords:** nanoparticles, Sumanene, Corannulene, Nanosheet, Anodes in Be-ion Batteries, M06-2X/6-31+G(d,p) method, cell voltage

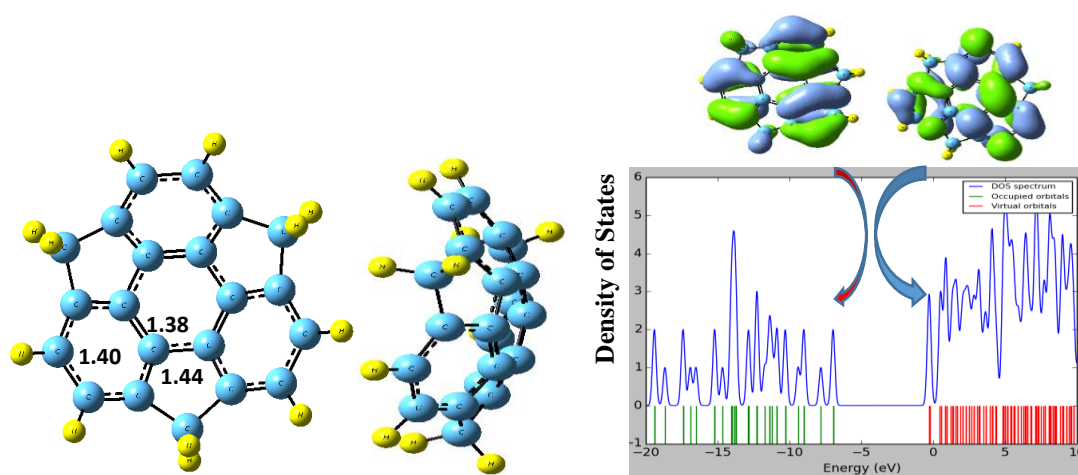
\*Corresponding Author: Tel.: 09360221112  
OR 09352357794 E-mail: [l\\_edjlali@iaut.ac.ir](mailto:l_edjlali@iaut.ac.ir)

## Introduction

Rechargeable batteries have been well investigated because of their capabilities to provide high energy density to power electronic devices for long-term utilization [1] Metal-ion batteries, especially Li-ion batteries (LIBs), have been widely investigated for flexible batteries due to their abilities to be built in an all-solid-state construction [2] Although the energy storage mechanisms between LIBs and supercapacitors are significantly different, the basic concepts to develop flexible batteries are similar [3]. TMC-based active materials [4] However, taking into account the nonaqueous electrolytes used in most rechargeable batteries, potential environmental and safety issues should be of concern to develop a human-compatible wearable device [5] The commercial and most typical Li-ion batteries are produced using layered materials as electrodes in which Li-ion intercalation/extraction processes are involved during discharge/charge cycling [6]. Li-Intercalation enables small volume expansion of active materials which ensures stable performance during long-term utilization, nevertheless, a low energy storage capacity is achieved [7]. Thereafter, novel electrode materials such as transition-metal based multi-valence materials based on other energy storage mechanisms such as alloying and conversion reactions have been developed to deliver much higher capacities than Li-intercalation electrodes, but the huge volume change becomes the major barrier to flexible batteries [8]. To address this issue, mechanically robust additives and self-adjusting nanostructures have been developed. [8–9] Similar to flexible SCs, carbon materials and CPs are commonly used to form a flexible and high conductivity network to load electrode materials for flexible LIBs [9]. Li-ion batteries utilize an intercalated lithium compound as the material at the positive electrode and typically graphite at the negative electrode. The batteries have a high energy density, high specific capacity, and the lowest electrochemical potential [10]. The most common combination is that of lithium cobalt oxide (cathode) and graphite (anode). Mesoporous  $\text{NiCo}_2\text{O}_4$  nanowire arrays coated with carbon textiles have been demonstrated to facilitate electron transport by directly connecting active materials to the current collectors and provide facile ion diffusion path by forming a mesoporous structure. Besides LIBs, other flexible metal-ion batteries such as Na-ion, Mg-ion, and Al-ion batteries have been developed in recent years. Besides experiencing similar challenges to flexible LIBs, other flexible batteries face problems in terms of sluggish metal ion diffusion in the electrodes and

limited options for electrode materials and electrolytes. A universal strategy to address these issues is to develop 3D electrodes with open channels in order to achieve the facilitated metal ion/cluster extraction and insertion from host materials to the electrolyte. However, the development of 3D electrodes for flexible Na-ion batteries is still hampered by the intricate production methods and the relatively high cost of building blocks for 3D structures such as graphene and CNTs. Polymer-based solid electrolytes can boost the development of highly safe and flexible Be-ion batteries because of great merits, including greatly improved safety, high energy density, and structural flexibility.

It can be proposed that Be-ion batteries (BeBs) may be adequate, replacement for NaBs because of the wide accessibility of Beryllium, its low expenditure and nontoxicity. Some of the nanoparticles are appropriate to use in metal-ion batteries, MIB [11–14]. Our the main goal of this article is the utilization of some carbon nanoparticles including sumanene (SM), corannulane (CN) and nanosheet with different structures in BeBs as an anode. Different interactions between  $\text{Be}^{2+}/\text{Be}$  and nanoparticles lead to different structures and obtain various cell voltages (Fig. 1). Sumanene can be synthesized by oxidation of 1, 5, 9-trimethyltriphenylene [15]. Corannulane was first prepared in 1966 by organic multistep synthesis [16-17]. In these different interactions was compared of the cell voltage (V) (Table 1). In this work, a report was made on computational studies of Be-ion batteries, which is useful for laboratory chemists.



[a]

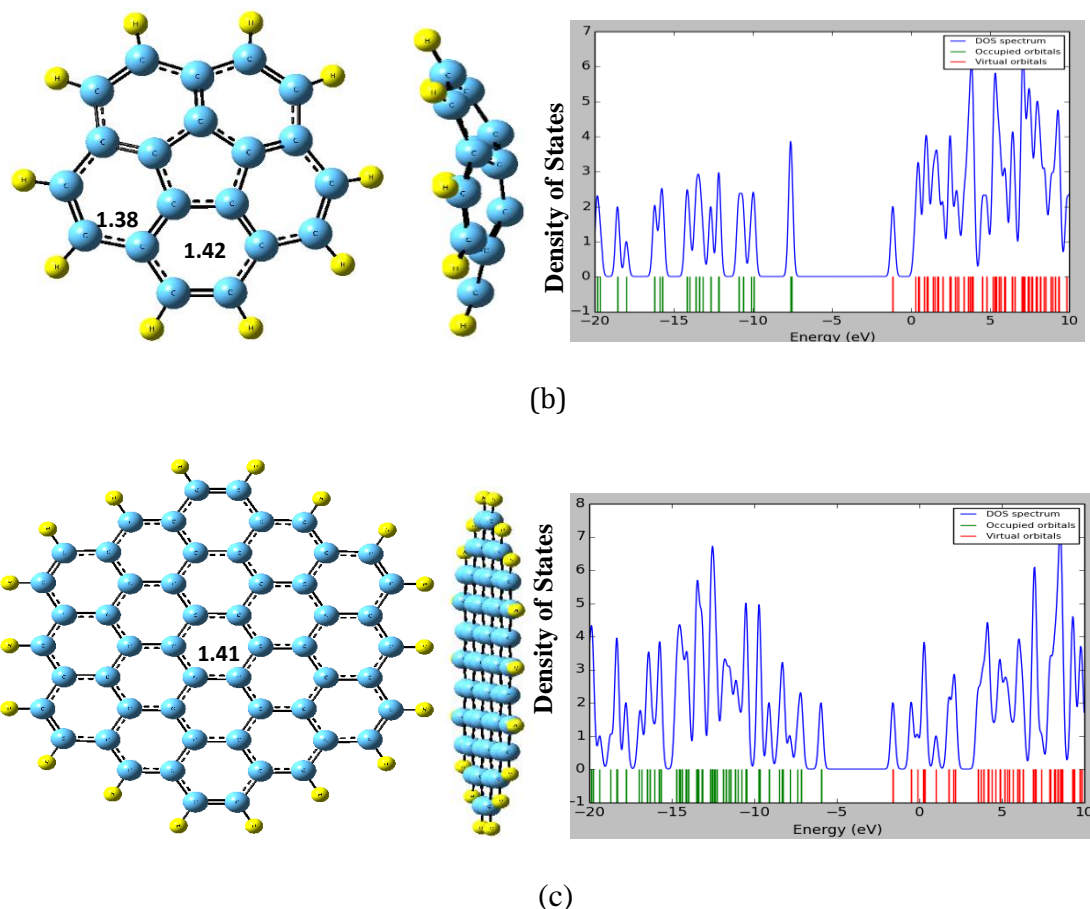


**Fig. 1.** Optimized molecular structures of (a) sumanene (SM); (b) corannulene (CN); (c) nanosheet

## 2. Computational methods

The geometries, adsorption energies and density of states (DOS) of monomers and complexes were fully optimised with the M06–2X level using 6–31+G (d, p) basis set [18]. The quantum chemical calculations carried out with the G09 program [19]. Vibrational frequencies were performed by the same level of theory to confirm that the structures obtained are local minima on the potential energy surface. The chemical compositions of the nanoparticles are SM,  $C_{21}H_{12}$ ; CN,  $C_{20}H_{10}$ ; and graphene,  $C_{54}H_{18}$ . Hydrogen atoms are application to cover the boundary carbon atoms of the nanoparticles. The natural bond orbitals (NBO) of the  $Be^{2+}/ Be$ -nanosheet complex were computed for the charge and hybridization study. The  $Be$  and  $Be^{2+}$  adsorption energy was performed on the basis of the optimised structures with the below equation:

$$E_{ad} = E_{complex} - E_{nanoparticle} - E_{Be/Be^{2+}} + E_{BSSE} \quad (1)$$

Where,  $E_{\text{nanoparticle}}$  is the energy of the nanoparticles including SM, CN and graphene. The  $E_{\text{complex}}$  is the energy of each nanoparticle which Be or  $\text{Be}^{2+}$  adsorbed on the surface. The  $E_{\text{BSSE}}$  relates to the basis set superposition error which is calculated by the counterpoise method of Boys and Bernardi [20].

The HOMO–LUMO energy gap ( $E_g$ ) is calculated as:

$$E_g = E_{\text{LUMO}} - E_{\text{HOMO}} \quad (2)$$

Where  $E_{\text{LUMO}}$  and  $E_{\text{HOMO}}$  are energies of HOMO and LUMO levels. The change of  $E_g$  is computed as follows:

$$\Delta E_g = [(E_{g2} - E_{g1})/E_{g1}] * 100 \quad (3)$$

Where,  $E_{g1}$  and  $E_{g2}$  are for nanostructures value and the complex value. This parameter indicates the electronic sensitivity of the nanoparticle to the  $\text{Be}^{2+}/\text{Be}$  adsorption. The Gausssum program has been used to compute the DOS plots [21].

### 3. Results and discussions

In here, three kinds of nanostructures were determined to study their interactions with Be atom and  $\text{Be}^{2+}$  ion. The cell voltage (V) of the three nanoparticles based Be–ion battery (NIBs) was calculated and discussed. All complexes were found in the global minima, which all regions at top of pentagon or hexagon ring for possible interaction with Be neutral atom and  $\text{Be}^{2+}$  ion.

#### 3.1 Adsorption of Be/ $\text{Be}^{2+}$ over the sumanene

the sumanene includes a benzene ring in the center and the boundary line in cyclopentadiene and benzene rings is shown in Fig. 1 [53]. Also it has six carbon atoms by  $9^\circ$  and range bond lengths range is from 1.38 to 1.43 angstrom are pyramidalized. SM has a bowl–shaped with a bowl depth of 1.18 angstrom [22]. The HOMO and LUMO energies are  $-6.95$  and  $-0.29$  eV, respectively; thus the HOMO–LUMO gap energy is 6.67 eV (Table 1). Also study the behavior of adsorption of Be/ $\text{Be}^{2+}$  on SM, we must study all possibilities of the interaction between Be/ $\text{Be}^{2+}$  and both inside or outside the bowl.

##### 3.1.1 Adsorption of Be/ $\text{Be}^{2+}$ outside the bowl of sumanene

$\text{Be}^{2+}$  and Be were optimized above the surface of the six-membered ring in sumanene with distances of  $3.50$  and  $3.27$  Å from carbon atoms, respectively is shown in Fig. 2. This indicates a good interaction between SM and both  $\text{Be}^{2+}$  ion and Be atom. From the comparison of the adsorption energy,  $E_{\text{ad}}$ , it can be seen that the  $\text{Be}^{2+}$  ion on the SM is  $-164.03\text{kcal mol}^{-1}$  that is larger than that of the Be atom ( $-1.91\text{kcal mol}^{-1}$ ) (Table 1). Higher interaction between SM and  $\text{Be}^{2+}$  ion related to an interaction between Lewis base and Lewis acid.

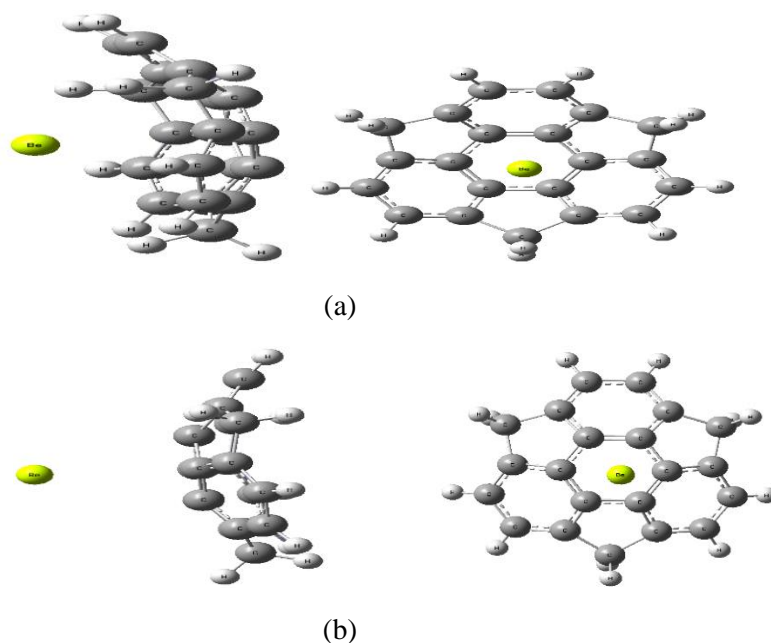


**Fig. 2.** Optimized structures of  $\text{Be}^{2+}$  and Be-SM complexes. (a)  $\text{Be}^{2+}$ -SM complex (b) Be-SM complex. Pink, green and blue balls are carbon, sodium and hydrogen atoms.

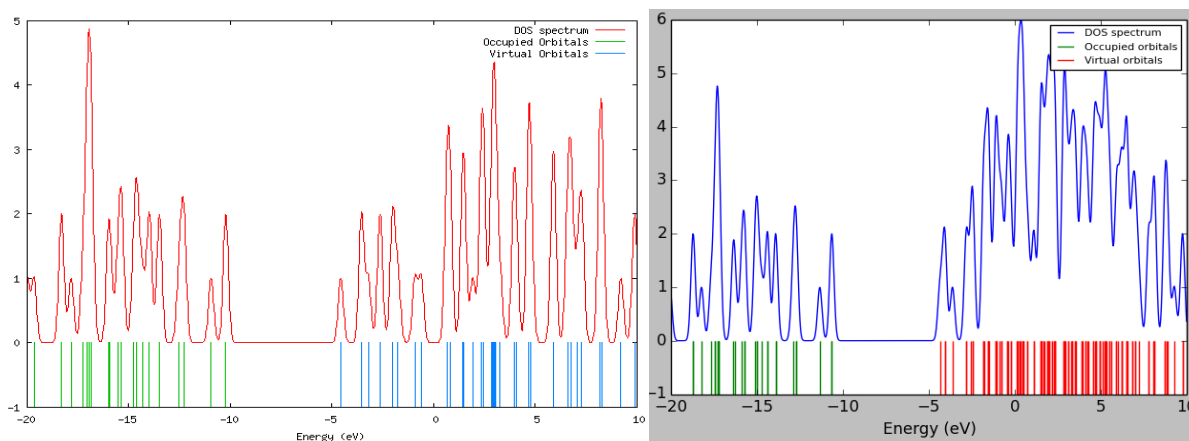
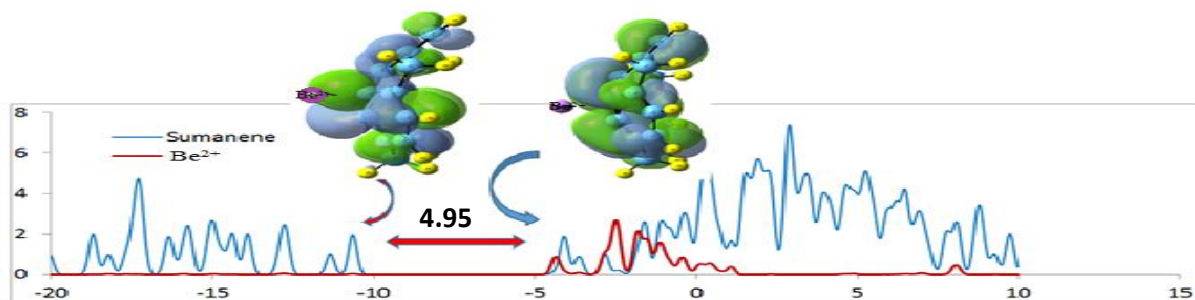


**Fig. 3.** Density of states (DOS) plot of SM (right) and  $\text{Be}^{2+}$ - SM complex (left).

The target of boundary molecular orbital analysis from the changes of the orbital level is to find which orbitals play main role in the interactions between nanoparticles and Be atom or  $\text{Be}^{2+}$  ion. The  $\% \Delta E_g$  to the lower energies for the  $\text{SM}-\text{Be}^{2+}$  complex (Fig. 3). The HOMO and LUMO levels due to of  $\text{Na}^+$  ion adsorption on SM at the most optimal point is sharp for LUMO level. The LUMO level mainly stabilized from  $-0.29$  eV in SM to  $-10.05$  eV in the  $\text{SM}-\text{Be}^{2+}$  complex (Table 1), cause to decrease in the  $E_g$  ( $\sim 34.74$ ) amount. The density of state (DOS) diagrams indicated in Fig. 3. The partial density of states, PDOS, evidently shows that a new level created at the  $E_g$  gap of pristine which arises from  $\text{Be}^{2+}$  cation;  $E_g$  is reduced in the  $\text{Be}^{2+}-\text{SM}$  complex (Fig. 4). The action of atomic Na adsorption on the electronic aspects of  $\text{SM}-\text{Be}$  is unlike from that of  $\text{SM}-\text{Be}^{2+}$ . The Be adsorption leads unstable because of being an unpaired electron in HOMO of the  $\text{SM}-\text{Be}$  complex. The amount of the HOMO level is changed from  $-6.95$  to  $-6.66$  eV. The energy amount of the LUMO level is slightly changed from  $-0.29$  to  $-0.46$  eV as illustrated in Table 1 and Fig. 4. The  $E_g$  in Be adsorption on SM is much more than that of the  $\text{Be}^{2+}$  adsorption. The partial density of states, PDOS, (Fig. 4) obviously shows that a new level formed at the  $E_g$  gap of pristine mostly arises from the Be atom which causes to decrease mainly in  $E_g$  of  $\text{Be}-\text{SM}$  complex.  $\text{Be}^{2+}-\text{SM}$  and  $\text{Be}-\text{SM}$ , the electronic charge transfer could be explained that a new level produced from  $\text{Be}^{2+}$  cation at the LUMO area leads to decrease in  $E_g$  of the  $\text{Be}^{2+}-\text{SM}$  complex as well as increase the electronic charge transfer from HOMO of SM to LUMO of  $\text{Be}^{2+}$  in the partials density of states (PDOS) plot. The electronic charge transfer for the  $\text{Be}-\text{SM}$  complex is more than the  $\text{Be}^{2+}-\text{SM}$  complex because the  $E_g$  for the  $\text{Be}-\text{SM}$  complex is less than the  $\text{Be}^{2+}-\text{SM}$  complex.



(a)

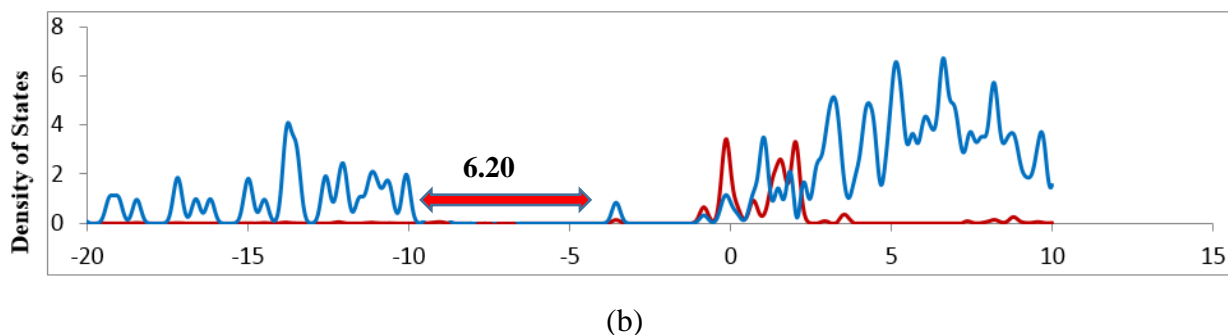


**Fig. 4.** Partial density of states (PDOS) plot of  $\text{Be}^{2+}$ -SM and Be-SM. (a) PDOS plot of  $\text{Be}^{2+}$ -SM (b) PDOS plot of Be-SM

The Density-functional theory (DFT) computational described that the  $p$  character of carbon atoms in the six-membered ring increases during adsorption of  $\text{Be}^{2+}$  since those carbon atoms intend to interact with the  $\text{Be}^{2+}$  cation. Strong interaction between  $\pi$  electrons of the six-membered ring and  $\text{Be}^{2+}$  cause to increase of the  $p$  character of carbon atoms and consequently to an increase of the bond length distance in  $\text{Be}^{2+}$ -SM complex.

### 3.1.2 Adsorption of Be/ $\text{Be}^{2+}$ inside the bowl of sumanene

The complexes between  $\text{Be}^{2+}$  ion and Be atom with six-membered ring inside the bowl of sumanene were formed at the optimal point. The adsorption energies,  $E_{\text{ad}}$ , of  $\text{Be}^{2+}$ -SM-i is  $-168.12 \text{ kcal mol}^{-1}$  that is larger than that of the Be atom ( $-9.76 \text{ kcal mol}^{-1}$ ) as illustrated in Table 1. The bond lengths between  $\text{Be}^{2+}$  ion and Be atom from carbon atom  $\text{C}1$  and  $\text{C}2$ ,  $\text{\AA}$ , respectively (Fig. 5). A appropriate interaction between  $\text{Be}^{2+}$ -SM-i and Be-SM-i inside the bowl of SM-i respect to outside the bowl of  $\text{Be}^{2+}$ -SM and Be-SM complex. The changes in the HOMO and LUMO levels and  $E_g$  for Be/ $\text{Be}^{2+}$  inside the bowl of SM-i is similar to outside the bowl of SM; stabilizing during  $\text{Be}^{2+}$  adsorption over SM-i which the stabilization is sharp for LUMO level. The LUMO level mainly stabilized from  $-0.29 \text{ eV}$  in SM-i to  $-10.32 \text{ eV}$  in the  $\text{Be}^{2+}$ -SM-i complex (Table 1); decreasing in the  $E_g$  ( $\sim 25.48\%$ ). The changes in HOMO, LUMO and  $E_g$  are illustrate in Fig. 6 by density of state (DOS) diagrams. The HOMO level changed from  $-6.95$  to  $-15.29 \text{ eV}$ . The energy of the LUMO level is slightly increased from  $-0.29$  to  $-10.32 \text{ eV}$  as shown in Table 1 and Fig. 6. As a result of large change in HOMO, the  $E_g$  is significantly

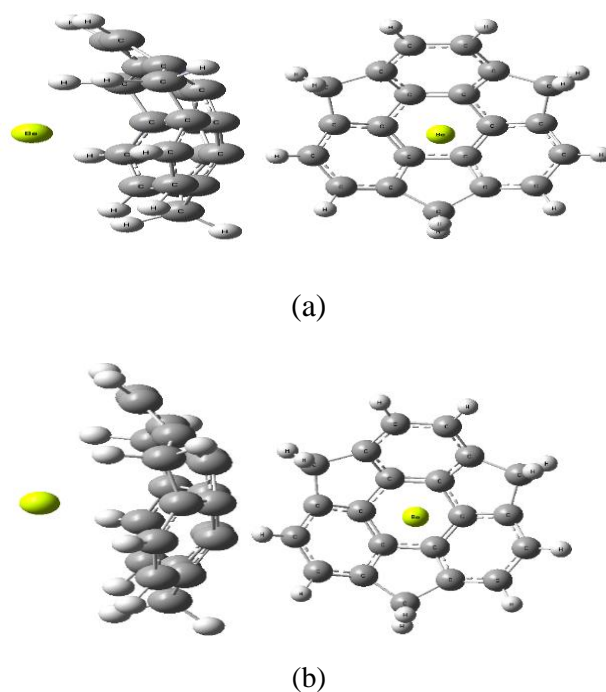


**Fig. 5.** Optimized structures of  $\text{Be}^{2+}$  and  $\text{Be-SM-i}$  complexes. (a)  $\text{Be}^{2+}$ -SM-i complex (b)  $\text{Be-SM-i}$  complex. Pink, green and blue balls are carbon, sodium and hydrogen atoms.

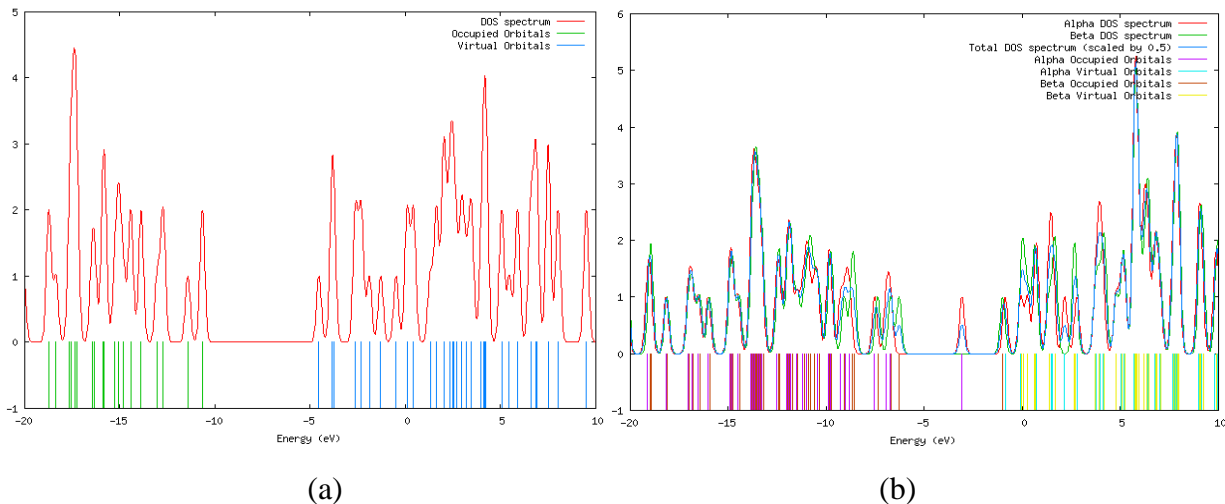


**Fig. 6.** Density of states (DOS) plot of (a)  $\text{Be}^{2+}$ - SM-I; (b)  $\text{Be-SM-i}$ .

narrowed by about -25.48%, indicating that the effect of Be adsorption on the  $E_g$  is much more than that of the  $\text{Be}^{2+}$  adsorption process.

### 3.1.3 Adsorption of $\text{Be}/\text{Be}^{2+}$ outside the bowl of corannulene

The corannulene nanoparticle composed by a cyclopentane ring fused with four benzene rings named as a bucky bowl. The CN nanoparticle have a bowl-to-bowl inversion with a barrier energy of 10.2 kcal/mol at  $-64\text{ }^{\circ}\text{C}$  [23]. The  $\text{Be}^{2+}$  ion and Be atom were interacted above the surface of the five-membered ring of CN with distances of  $1.01$  and  $1.19\text{ \AA}$  from carbon atom, respectively (Fig. 7). The adsorption energy,  $E_{\text{ad}}$ , of the  $\text{Be}^{2+}$  ion on the CN is  $-165.89\text{ kcal mol}^{-1}$  that is higher than that of the Be neutral ( $-2.01\text{ kcal mol}^{-1}$ ) (Table 1). The interactions between CN and both  $\text{Be}^{2+}$  ion and Be neutral are stronger than those of surname.

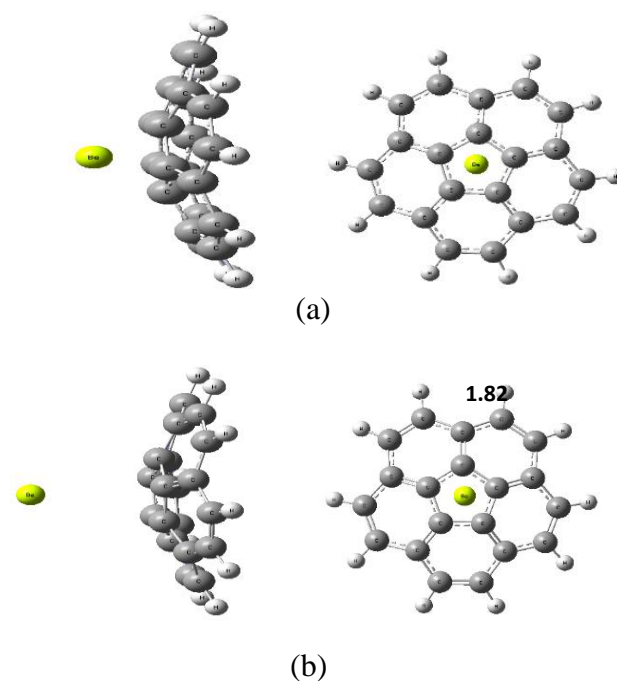


**Fig. 7.** Optimized structures of  $\text{Be}^{2+}$  and Be-CN complexes. (a)  $\text{Be}^{2+}$ -CN complex (b) Be-CN complex, Distances are in  $\text{\AA}$ . Pink, green and blue balls are carbon, sodium and hydrogen atoms.

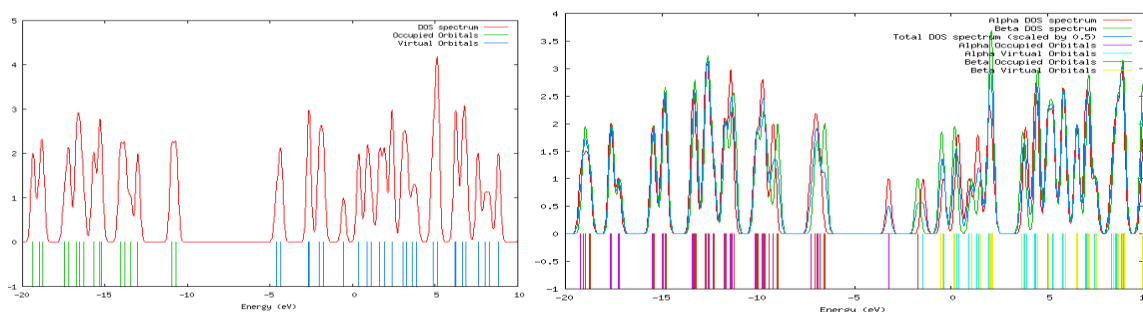


**Fig. 8.** Density of states (DOS) plot of (a)  $\text{Be}^{2+}$ -CN; (b) Be-CN.

The  $\Delta E_g$  to the lower energies (more negative) for the CN-Be<sup>2+</sup> complex (Fig. 8) which shifting is sharp for LUMO level. The LUMO level considerably stabilized from -1.14 eV in CN to -10.26 eV in the CN-Be<sup>2+</sup> complex (Table 1), leading to decrease in the  $E_g$  ( $\sim -32.91\%$ ). The  $\Delta E_g$  and  $E_g$  are shown in Fig. 4 by density of state (DOS) diagrams. The density of states, DOS, obviously explains that a new peak formed at the  $E_g$  gap of pristine mostly arises from Be<sup>2+</sup> cation which leads to diminish in  $E_g$  of the Be<sup>2+</sup>-CN complex (Fig. 8). The Be adsorption over CN the HOMO level is changed from -7.56 for CN to -6.62 eV. The shape of HOMO is changed remarkably by transferring to the adsorbing region. The energy of the LUMO level is shown in Table 1 and Fig. 8. The  $E_g$  is significantly decreased by -25.48%, indicating that the Be adsorption changes the  $E_g$  much more than that of the Be<sup>2+</sup> adsorption. The changes in HOMO, LUMO and  $E_g$  are to put forthed in Fig. 8 using density of state (DOS) diagrams.

### 3.1.4 Adsorption of Be/Be<sup>2+</sup> inside the bowl of corannulene

The Be<sup>2+</sup> ion and Be atom were optimized inside the plane of the five-membered ring of CN with distances of 1.24 and 1.34 Å, respectively (Fig. 9). The adsorption energy,  $E_{ad}$ , of the Be<sup>2+</sup> ion inside the CN is -167.00 kcal mol<sup>-1</sup> that is higher than that of the Be neutral (-8.72 kcal mol<sup>-1</sup>) (Table 1).

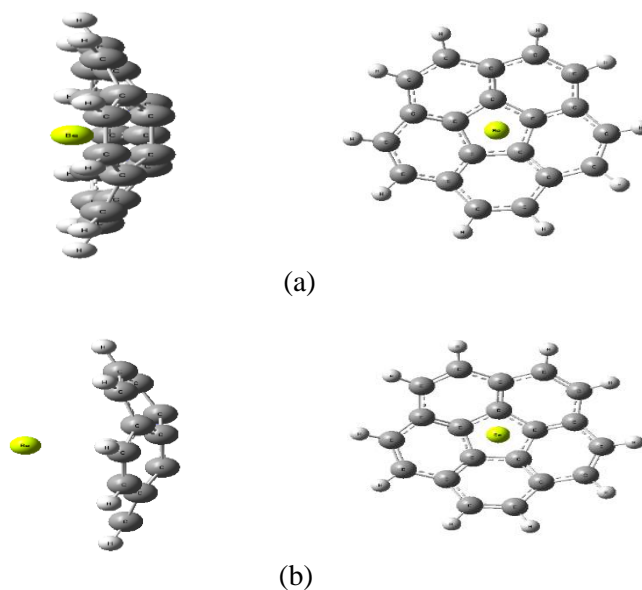
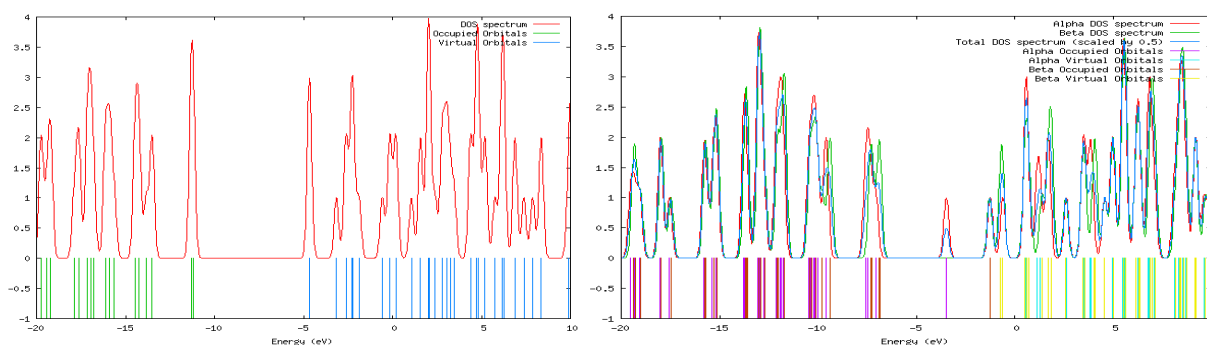


Fig. 9. Optimized structures of Be<sup>2+</sup> and Be-CN-i complexes. (a) Be<sup>2+</sup>-CN-i complex (b) Be-CN-i complex. Pink, green and blue balls are carbon, sodium and hydrogen atoms.

The changes in the HOMO and LUMO levels and  $E_g$  for Be/Be<sup>2+</sup> inside the bowl of corannulene is approximately similar to outside the bowl of corannulene. The LUMO level noticeably stabilized from  $-1.14$  eV in CN to  $-10.72$  eV in the Be<sup>2+</sup>-CN-i complex (Table 1); causing to diminish in the  $E_g$  ( $\sim 36.30\%$ ). The changes in HOMO, LUMO and  $E_g$  are illustrate in Fig. 10 by density of state (DOS) diagrams. This HOMO level is changed from  $-7.56$  for CN to  $-2.29$  eV for Be-CN-i complex which is singly occupied. The energy of the LUMO level is almost slightly changed from  $-1.14$  to  $-1.20$  eV as shown in Table 1 and Fig. 10. The  $\Delta E_g$  is about  $-36.30\%$ , indicating that the effect of Be<sup>2+</sup> adsorption on the  $E_g$  is much more than that of the Be adsorption process.



**Fig. 10.** Density of states (DOS) plot of (a) Be<sup>2+</sup>-CN-i; (b) Be-CN-i.

### 3.1.5 Adsorption of Be/Be<sup>2+</sup> over nanosheet

The Be<sup>2+</sup> ion and Be atom were optimized above the plane of the six-membered ring of nanosheet with distances of 1.16 and 3.20 Å, respectively (Fig. 11). The adsorption energy,  $E_{ad}$ , of the Be<sup>2+</sup> ion on the nanosheet is  $-169.93$  kcal mol<sup>-1</sup> that is larger than that of the Be neutral ( $-12.03$  kcal mol<sup>-1</sup>) (Table 1).

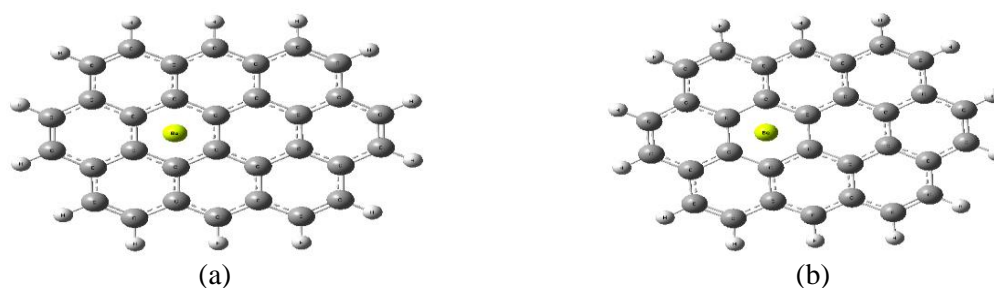


**Fig. 11.** Optimized structures of Be<sup>2+</sup> and Be-Sheet complexes. (a) Be<sup>2+</sup>-Sheet complex (b) Be-Sheet complex, Distances are in Å. Pink, green and blue balls are carbon, sodium and hydrogen atoms.

The HOMO and LUMO levels for nanosheet changes to the lower energies for the nanosheet–Be<sup>2+</sup> complex (Fig. 12). The LUMO level from –1.59 eV in nanosheet to –9.27 eV in the nanosheet–Be<sup>2+</sup> complex (Table 1). The changes in HOMO, LUMO and E<sub>g</sub> are illustrate in Fig. 12 by density of state (DOS). Amount of the HOMO level of the Be adsorption on nanosheet is changed from –5.95 to –6.03 eV. The energy of the LUMO level is slightly changed as shown in Table 1. The E<sub>g</sub> is significantly decreased by -62.74%, representing that the Be adsorption changes the E<sub>g</sub> more than that of the Be<sup>2+</sup> adsorption. The changes in HOMO, LUMO and E<sub>g</sub> are demonstrated in Fig. 12 using density of state (DOS).

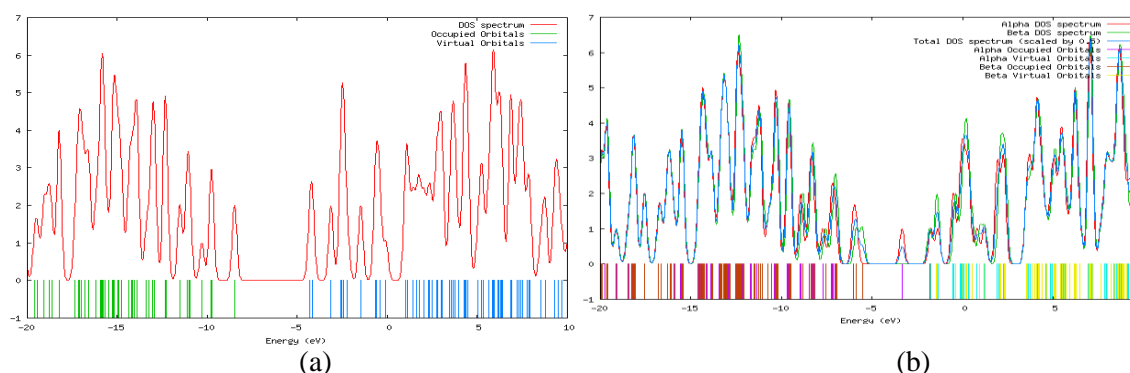


**Fig. 12.** Density of states (DOS) plot of (a) Be<sup>2+</sup>– Sheet; (b) Be–Sheet.

**Table 1.** The adsorption energies of atomic Be and Be<sup>2+</sup> (E<sub>ad</sub>, kcalmol<sup>-1</sup>) on different nanostructures.

Nanoparticle	E <sub>ad</sub>	E <sub>HOMO</sub>	E <sub>LUMO</sub>	E <sub>g</sub>	%ΔE <sub>g</sub>	ΔE <sub>cell</sub>	V <sub>cell</sub>
SM	---	-6.95	-0.29	6.67	---	---	---
SM/Be	-1.91	-6.66	-0.46	6.20	-7.58	---	---
SM/Be <sup>2+</sup>	-164.03	-15.00	-10.05	4.95	-34.74	-162.12	-7.04
SM-i/ Be	-9.76	-6.70	-0.41	6.29	-6.04	---	---
SM-i/ Be <sup>2+</sup>	-168.12	-15.29	-10.32	4.97	-25.48	-149.19	-6.483
CN	---	-7.56	-1.14	6.42	---	---	---
CN / Be	-2.01	-6.62	-1.23	5.39	-16.04	---	---
CN/ Be <sup>2+</sup>	-165.89	-15.09	-10.26	4.83	-32.91	-163.88	-7.121
CN -i/ Be	-8.72	-6.66	-1.20	5.46	-17.58	---	---
CN -i/Be <sup>2+</sup>	-167.00	-15.43	-10.72	4.71	-36.30	-146.28	-6.35
Sheet	---	-5.95	-1.59	4.36	---	---	---
Sheet/Be	-12.03	-6.03	-1.44	7.47	-62.74	---	---
Sheet/ Be <sup>2+</sup>	-169.93	-12.63	-9.27	3.36	-36.60	-157.9	-6.86

Energies of HOMO, LUMO, and HOMO–LUMO gap (E<sub>g</sub>) in eV. ΔE<sub>g</sub> indicates the change of E<sub>g</sub> of nanoparticles after the Be/Be<sup>2+</sup> adsorption. The total energy change (ΔE<sub>cell</sub>, kcal mol<sup>-1</sup>) and cell voltage (V) of the nanoparticles based Be–ion battery.

### 3.2. Comparison the nanoparticles in the Be<sup>2+</sup>-ion batteries (BeBs)

Three kinds of nanoparticles proposed as an anode for the BeBs. The typical reactions in the anode and cathode are the following process [24]:



This reaction can be divided into several reactions that are presented below:



The total reaction of the cell can be defined as:



The Nernst equation is used to obtain the cell voltage ( $V_{\text{cell}}$ ) as follows:

$$V_{\text{cell}} = -\Delta G_{\text{cell}}/zF \quad (7)$$

where,  $F$  and  $z$  are the Faraday constant ( $96500 \text{ Cmol}^{-1}$ ) and charge of  $\text{Be}^{2+}$  ( $z=2$ , the cation in electrolyte), respectively. The  $\Delta G_{\text{cell}}$  is the Gibbs free energy difference of the total reaction of cell. For DFT calculations at 0 K, it can be presented:

$$\Delta G_{\text{cell}} = \Delta E_{\text{cell}} + P\Delta V - T\Delta S \quad (8)$$

Theoretical storage capacity was achieved by comparing two relative interaction energies. One interaction energy is related to interaction between the  $\text{Be}^{2+}$  ion and nanoparticle which strong interaction energy leads to high cell voltage. Another interaction energy is related to interaction between the Be atom and nanoparticle which weak interaction energy leads to high cell voltage.

In previous reports we assume that the amount of volume and entropy contribution are very small ( $< 0.01 \text{ V}$ ) to the  $V_{\text{cell}}$  [25]. Therefore, the  $V_{\text{cell}}$  for  $\text{Be}^{2+}$ - or Be-nanoparticle can be determined by calculating the internal energy change ( $\Delta E$ ) from Eqs. 6 and 8 as follows:

$$\Delta E_{\text{cell}} \sim \Delta G_{\text{cell}} = E_{\text{Be}} + E_{\text{Be}^{2+}\text{-nanoparticle}} - E_{\text{Be}^{2+}} - E_{\text{Be-nanoparticle}} \quad (9)$$

Eq. 9 indicates that the strong interaction between  $\text{Be}^{2+}$  and nanoparticle and weak interaction between Be atom and nanostructure obtain more negative and high  $\Delta E_{\text{cell}}$ . In conclusion, the strong adsorption of  $\text{Be}^{2+}$  and weak adsorption of Be on the nanoparticle lead to high  $V_{\text{cell}}$  (Table 1). The adsorption energy between  $\text{Be}^{2+}$  and nanostructures,  $E_{\text{ad}}$ , is increased in the order: Sheet  $>$  SM-i  $>$

CN-i > CN > SM. The  $\Delta E_{\text{cell}}$ , and  $V_{\text{cell}}$  are calculated for three nanoparticles which presented in Table 1 and schemed in Fig. 13. The  $\Delta E_{\text{cell}}$ , and  $V_{\text{cell}}$  values for three nanoparticles in BeBs changed in the same order: CN > SM > Sheet > SM-i > CN-i. The largest  $\Delta E_{\text{cell}}$  and  $V_{\text{cell}}$  values of  $-163.88$  kcal/mol and  $7.21$  V, respectively, belonged to CN. The  $V_{\text{cell}}$  for CN is the highest because the interaction between SM and the Be neutral is the lowest. The strong interaction between  $\text{Be}^{2+}$  and nanoparticle and the weak interaction between the Be atom and nanoparticle lead to higher  $V_{\text{cell}}$  amount of the BeBs–nanoparticle. The  $\Delta E_{\text{cell}}$  and  $V_{\text{cell}}$  for BeBs–nanosheet are  $-157.90$  kcal/mol and  $-6.86$  V, respectively, which are lower than the values of CN. The lowest  $V_{\text{cell}}$  value belongs to the BeBs–CN–i due to highest interaction between the Be neutral and CN–i. In general, the  $V_{\text{cell}}$  value for BeBs– nanoparticles are from  $-146.28$  to  $-6.35$  V, makes these nanostructures the promising candidates which could use to manufacture of the BeBs as anode. We can report that the interaction between the Be neutral and nanostructures play a significant role in  $V_{\text{cell}}$  respect to the interaction between the  $\text{Be}^{2+}$  neutral and nanostructures.

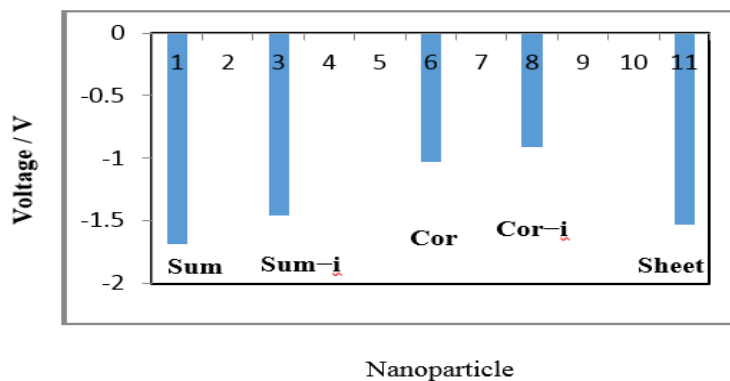


**Fig. 13.** The diagram of the cell voltage vs. different nanostructures as an anode of Be ion batteries, BeBs.

#### 4. Conclusions

In this research, the adsorption of  $\text{Be}^{2+}$  and Be over three types of the nanoparticles including sumanene (Sum), corannulene (CN) and nanosheet was studied to scrutinize their possible application as an anode of BeBs. The interaction between  $\text{Be}^{2+}$  and the surface of nanoparticles is clearly stronger than that of the Be which clarifies that these nanoparticles are appropriate as an anode of BeBs. The energy adsorption,  $E_{\text{ad}}$ , between  $\text{Be}^{2+}$  and nanosheet was the highest adsorption energy which  $E_{\text{ad}}$  were changed in the order: Sheet > Sum-i > CN-i > CN > Sum. However, the cell voltage,  $V_{\text{cell}}$ , was the highest for sumanene. The changes

in  $V_{\text{cell}}$  of BeBs are in the order: CN > Sum > Sheet > Sum-i > CN-i. The interaction between  $\text{Be}^{2+}$  and Be and nanoparticles play a remarkable role in determination of the cell voltage. The strong interaction between  $\text{Be}^{2+}$  and nanoparticles and weak interaction between Be and nanoparticles led to obtain a high  $V_{\text{cell}}$ .

## References

- [1] M. Winter, B. Barnett and K. Xu, *Chem. Rev.*, 118(23), 11433–11456 (2018).
- [2] J.L. Shi, D.D. Xiao, M. Ge, X. Yu, Y. Chu, X. Huang, X.D. Zhang, Y. X. Yin, X. Q. Yang, Y. G. Guo, L. Gu and L. J. Wan, *Adv. Mater.*, 30(9), 1705575 (2018).
- [3] B. K. Peters, K. X. Rodriguez, S. H. Reisberg, S. B. Beil, D. P. Hickey, Y. Kawamata, M. Collins, J. Starr, L. Chen, S. Udyavara, K. Klunder, T. J. Gorey, S. L. Anderson, M. Neurock, S. D. Minter and P. S. Baran, *Science.*, 363(6429), 838–845 (2019).
- [4] J. B. Goodenough, *Nat. Electron.*, 1(3), 204–204 (2018).
- [5] M. R. Palacín, *Chem. Soc. Rev.*, 47(13), 4924–4933 (2018).
- [6] P. K. Nayak, E. M. Erickson, F. Schipper, T. R. Penki, N. Munichandraiah, P. Adelhelm, H. Sclar, F. Amalraj, B. Markovsky and D. Aurbach, *Adv. Energy Mater.*, 8(8), 1702397 (2018).
- [7] C. Zhan, T. Wu, J. Lu and K. Amine, *Energy Environ. Sci.*, 11(2), 243–257 (2018).
- [8] H. Zhang, I. Hasa and S. Passerini, *Adv. Energy Mater.*, 8(17), 1702582 (2018).
- [9] K. Liang, K. Marcus, Z. Yang, L. Zhou, H. Pan, Y. Bai, Y. Du, M. H. Engelhard and Y. Yang, *Small*, 14(3), 1702295 (2018).
- [10] W. Xu, J. Wang, F. Ding, X. Chen, E. Lisybulin, Y. Zhang, J.G. Zhang, *Energy Environ. Sci.*, 7, 513–537 (2014).
- [11] A. Hosseinian, E. Saedi Khosroshahi, K. Nejati, E. Edjlali, E. Vessally, *J. Mol. Model.*, 23, 354 (2017).
- [12] K. Nejati, A. Hosseinian, L. Edjlali, E. Vessally, *J. Mol. Liq.*, 229, 167–171(2017).
- [13] P. Subalakshmi, A. Sivashanmugam, *J. Alloys Compd.*, 690, 523–531(2017).
- [14] K. Nejati, A. Hosseinian, A. Bekhradnia, E. Vessally, L. Edjlal, *J Mol Graph Model.*, 74, 1–7(2017).
- [15] H. Sakurai, T. Daiko, T. Hirao, *Science.*, 301, 1878–1878 (2003).
- [16] W. E. Barth, R.G. Lawton, *J. Am. Chem. Soc.*, 88, 380–381 (1966).
- [17] R. G. Lawton, E. W. Barth, *J. Am. Chem. Soc.*, 93, 1730–1745 (1971).

- [18] J. D Chai, M. Head–Gordon, *Phys. Chem. Chem. Phys.*, 10, 6615 (2008).
- [19] M. J. Frisch, et. Al, Gaussian09 program, (Gaussian Inc.,WalNangford, CT, 2009).
- [20] S.F. Boys, F. Bernardi, *Mol. Phys.*, 19, 553–561 (1970).
- [21] N. O’Boyle, A. Tenderholt, K. Langner, *J. Comput. Chem.*, 29,839–845 (2018).
- [22] S. Hidehiro, D. Taro, S. Hiroyuki, A. Toru, H. Toshikazu, *J. Am. Chem. Soc.*, 127 , 11580 –11581, (2005).
- [23] L.T. Scott, M. M. Hashemi, M. S. Bratcher, *J. Am. Chem. Soc.*, 114 (5) 1920–1921 (1992).
- [24] P. A. Denis, F. Iribarne, *Chem. Phys. Lett.*, 573, 15–18 (2013).
- [25] Z. Gao, C. S. Chin, J. H. K. Chiew, J.J.C. Zhang, *Energy.*, 10, 1503 (2017).

#### How to Cite This Article

Fatemeh Gharibzadeh, Esmail Vessally, Ladan Edjlali, Moosa Es’haghi, Robab Mohammadi , “A density functional theory study on nanostructures including sumanene, corannulene and nanosheet as the anodes in Be–ion Batteries” *International Journal of New Chemistry.*, 2021, 8(4), 425-441; DOI: 10.22034/ijnc.2021.528323.1158.